7

Carbon Redox Chemistry: Deep Carbon Dioxide and Carbonates

Choong-Shik Yoo

ABSTRACT

Carbon dioxide is an important terrestrial volatile, often considered to exist in deep Earth interior, and it plays a critical role in the deep carbon cycle. Yet it is not well understood whether or how such volatile carbon species are incorporated into the Earth's lower mantle and core. Here, we present the phase/chemical diagram of carbon dioxide that signifies the transformation of molecular CO_2 to extended solids, ionic carbonates, and ultimately its elemental decomposition products of C and O_2. We also discuss fundamental barochemical concepts governing carbon redox processes that may occur to recycle carbonaceous species in deep Earth's interior.

7.1. INTRODUCTION

Carbon dioxide exists in the atmosphere (as a major greenhouse gas), the ocean, and near the surface of Earth's crust, primarily as carbonates such as calcite and dolomite (Zhu & Ogasawara, 2002). It is also considered to exist deep in the Earth's mantle (Saal et al., 2002) and play a critical role in the deep carbon cycle (Hazen et al., 2013). The presence of carbon dioxide deep in Earth's interior is apparent from its abundance in magma plumes (Schrauder & Navon, 1993) and from assemblages of carbonate minerals such as aragonite and magnesite (Isshiki et al., 2004). In various thermal and chemical conditions, carbon dioxide converts to a wide variety of carbonaceous species, including diamond, graphite, carbon monoxide, and carbonates. Thus, the transformation of carbon, carbon dioxide, and carbonates at high pressures and temperatures is critical to understanding the origin of deep carbon, carbon budget, and carbon cycle (Hazen et al., 2013; Mao et al., 2003; Sleep et al., 2001).

Chemistries and properties of carbonaceous volatiles such as C, CO, CO_2, and carbonates are not well understood at high pressures and temperatures (P-T). Yet, it is not well understood whether or how such volatile species are incorporated into the Earth's lower mantle and core, resulting in a major uncertainty in the deep carbon cycle. The presence of CO_2 deep in the Earth can alter the properties of minerals and rocks, including the melting temperature and mechanical strength and, thereby, strongly affect the chemical and physical stability of deeply subducting plates (Dasgupta & Hirschmann, 2006; Kelemen & Manning, 2015). The mass and thermal diffusion rates of carbon dioxide into rocks and minerals are important considerations for carbon dioxide sequestration (Kampman et al., 2014; Leckner, 2003), but they are largely unknown at elevated P-T conditions, leaving questions about long-term storages in depleted oil and gas reservoirs. The relative stabilities of carbonate minerals (such as calcite $CaCO_3$, magnesite $MgCO_3$, and siderite $FeCO_3$) with respect to the mixtures of high-density extended CO_2 (polymeric CO_2 or simply XCO_2) and minerals (such as CaO, MgO, and Fe) are not well understood. Yet they are important in understanding both the deep mantle presence of volatile species like CO_2 and their geochemical transportation mechanisms. Importantly, the chemistry of CO_2 with other volatiles like H_2, H_2O, or hydrous minerals is a primitive redox process, which can produce hydrocarbons and other simple organics and drive their evolutions.

Because of the significance of carbon dioxide in geochemistry, geological processes, and the deep carbon cycle, it is important to understand the phase and chemical behaviors of carbon dioxide at high P-T. Hence, we review

Department of Chemistry and Institute of Shock Physics, Washington State University, Pullman, Washington, USA

Carbon in Earth's Interior, Geophysical Monograph 249, First Edition. Edited by Craig E. Manning, Jung-Fu Lin, and Wendy L. Mao.

the phase/chemical diagram of carbon dioxide and present four governing, fundamental transformations: (A) carbon oxidation, (B) carbonate formation, (C) ionization of extended CO_2, and (D) pressure-induced amorphization. These results indicate a large P-T stability domain of extended CO_2 and ionic carbonates, providing a geochemical mechanism for the origin of deep carbon species in the Earth's core and mantle boundary.

7.2. EXPERIMENTAL METHOD

The experiments were performed using laser-heated diamond anvil cells (DACs) coupled with confocal micro-Raman spectroscopy. Carbon dioxide samples were loaded into DACs from a liquid by condensing CO_2 gas to –35 °C and 15 atmospheres. Type IA diamond anvils were used with a flat culet size of 0.3 mm (or 0.1 mm) for higher pressures). A rhenium gasket was preindented to 0.04–0.05 mm in thickness, and a small hole of 0.12 (or 0.06) mm was drilled using an electric-discharge micro-drilling machine. A thin metal foil (Fe, Pt or B) (~0.01 mm) or a small piece of graphite was placed in the sample chamber to absorb the CW Nd: YLF laser (λ = 1054 nm) light and heat the CO_2 sample. The temperature of the sample was determined by measuring thermal emission and then fitting it for a gray-body Planck radiation equation. The pressure of the sample was measured using the Ruby luminescence method (Mao et al., 1986). Existences and transitions of different carbon dioxide phases were determined based on their characteristic Raman spectra.

7.3. RESULTS

The phase diagram of carbon dioxide is rather intricate, with an array of polymorphs exhibiting great diversity in crystal structure, chemical bonding, and collective interaction (Figure 7.1) (Yoo et al., 2011). At pressures above 40 to 60 GPa and temperatures of 300 to 1000 K, carbon dioxide transforms into a wide range of silicate-like extended solids (or XCO_2): four-fold CO_2-V, pseudo-six-fold CO_2-VI, coesite-like c-CO_2, amorphous *a*-carbonia, and ionic carbonate solid *i*-CO_2, all in high density between 3.5 and 3.8 g/cm^3. These are fundamentally new solids, consisting of monolithic 3D network structures of carbon atoms covalently bonded with oxygen atoms, largely in CO_4 tetrahedra (or orthocarbonates) similar to those of silicate minerals. These solids exhibit novel properties such as extremely low compressibility (Datchi et al., 2012; Yoo et al., 1999), strong optical nonlinearity (Iota et al., 1999), and presumably high melting temperatures (as in the case of diamond). The large disparity in chemical bonding between the extended network and molecular CO_2, on the other hand, allows these extended solids to exist over a large pressure domain (down to a few GPa), which provides opportunities for synthesis of novel materials.

To a first approximation, the crystallographic similarities between these extended CO_2 phases and SiO_2 polymorphs seem to indicate a periodic analogy between CO_2 and SiO_2 (Sengupta et al., 2010). Yet, unlike SiO_2, the polymerization of CO_2 accompanies a great level of modification in chemical bonding from weak van der Waals in

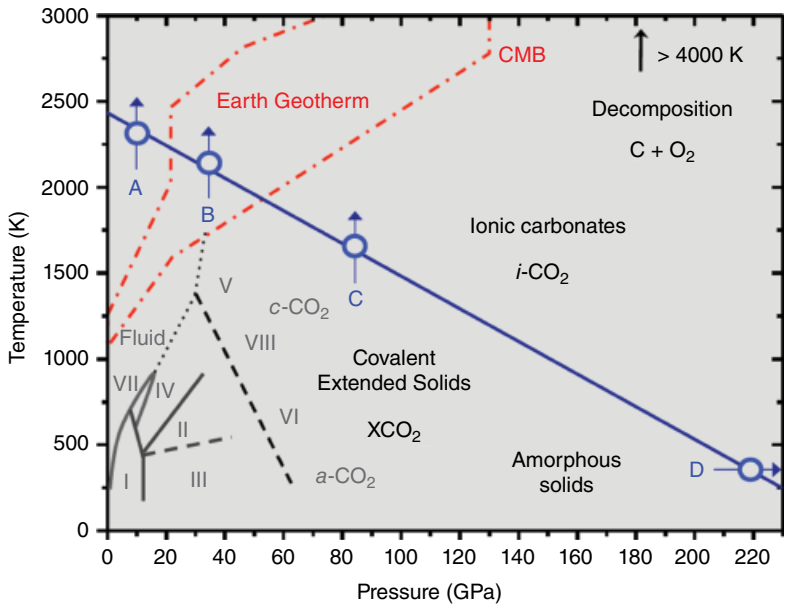

Figure 7.1 Phase and chemical transformation diagram of carbon dioxide, signifying the deep carbon cycle from molecular CO_2 phases to extended CO_2 solids (noted as XCO_2), ionic solids (i-CO_2) and, ultimately, decomposition products of C+O_2 at elevated temperatures and pressures. The blue line signifies the pressure (and temperature)–induced ionization of CO_2 phases, established by the specific transformations along the four blue arrows and described in sections 7.3.1 through 7.3.4. See electronic version for color representation of the figures in this book.

molecular solids (CO_2-I, CO_2 -III, and CO_2 -VII) to strong covalent bonds in extended CO_2. As a result, the phase diagram of carbon dioxide shows several thermal-path dependent phases (e.g., phase VI, c-coesite, and to an extent phase II and IV) and phase boundaries, underscoring the metastability and kinetics over a large P-T domain, making it difficult to determine the exact location of phase boundaries either experimentally or theoretically (Yoo, 2013).

Extended CO_2-V exhibits a stability over a large P-T domain: to 2000 K at 60 GPa and to 200 GPa at ambient temperature, above which it transforms to extended ionic solids (i-CO_2 or $COCO_3$) in the structure similar to post-aragonite $CaCO_3$ (Ono et al., 2005) and, ultimately, decomposes to elemental solids of carbon and oxygen at extreme temperatures above 4000 K (according to the previous shock wave studies (Nellis et al. 1991). Recently, the stability of CO_2-V has been reported even for a large P-T space well into the ionization line in Figure 7.1 (Dziubek et al., 2018), which may suggest a strong kinetic barrier associated with the transition. The presence of extended covalent (XCO_2) and ionic (i-CO_2) solids over a large P-T regime that overlaps with the Earth geotherm has significant implications to understanding the geochemistry of carbonaceous volatiles (C, CO, CO_2, and carbonates) and deep Earth's carbon cycle. Hence, described in sections 7.3.1 through 7.3.4 are governing carbon transformations along the specific thermal paths marked with arrows in Figure 7.1.

7.3.1. Carbon Oxidation

Carbon dioxide molecules are extremely stable at low pressures below 20 GPa, even to high temperatures above 3000 K. This is in contrast to the polymerization of CO_2 above 40 GPa. It clearly indicates the presence of a strong kinetic barrier for breaking C=O bonds at low pressures than at high pressures. In fact, CO_2-V can be made at a substantially lower pressure than 20 GPa, by heating phase IV in the presence of Ti catalyst (Sengupta et al., 2012). The polymerization of CO_2 is, on the other hand, an oxidation process converting sp^2 hybridized carbon in C=O to sp^3 carbon in C-O. As such, it is thought that the presence of oxygen can assist carbon oxidation and the formation of new CO_2 phases, especially at high temperatures. Figure 7.2 shows the catalytic reaction between hot carbon particles and oxygen molecules, producing CO_2 and $CO^{2+}CO_3^{2-}$, an ionic form of $(CO_2)_2$ at 2300 K and 8 GPa. The spectral evidence includes the characteristic vibrational peaks of CO_3^{2-} at 740 and 1075 cm^{-1} and CO^{2+} at 2230 cm^{-1} for $COCO_3$, and the Fermi resonance ν_- and ν_+ peaks of CO_2 on either sides of the diamond Raman peak at ~1335 cm^{-1}. Similar ionization reactions have previously been observed in nitrogen dioxide dimer (N_2O_4) both at high P-T (Agnew et al., 1983) and at ambient pressure and low temperature (Bolduan et al., 1984). It transforms to $NO^+NO_3^-$, whose vibrational spectrum is analogous to that of $COCO_3$. Figure 7.3 shows a striking similarity in lattice vibrations between $COCO_3$ and $NONO_3$ as an example.

These results clearly indicate the occurrence of carbon oxidation: $C + O_2 \rightarrow CO_2 \rightarrow COCO_3$ at relatively low pressures and high temperatures, thus overcoming the kinetic barrier. Note that $COCO_3$ is still a molecular ionic phase in contrast to extended ionic phase i-CO_3 formed at substantially higher pressure above 80 GPa (see Figure 7.1 and discussion in section 7.3.3). Nevertheless, the transformation occurs at the onset of the same phase line (the blue line in Figure 7.1), underscoring high stability of ionic solids over a large P-T region of the Earth mantle

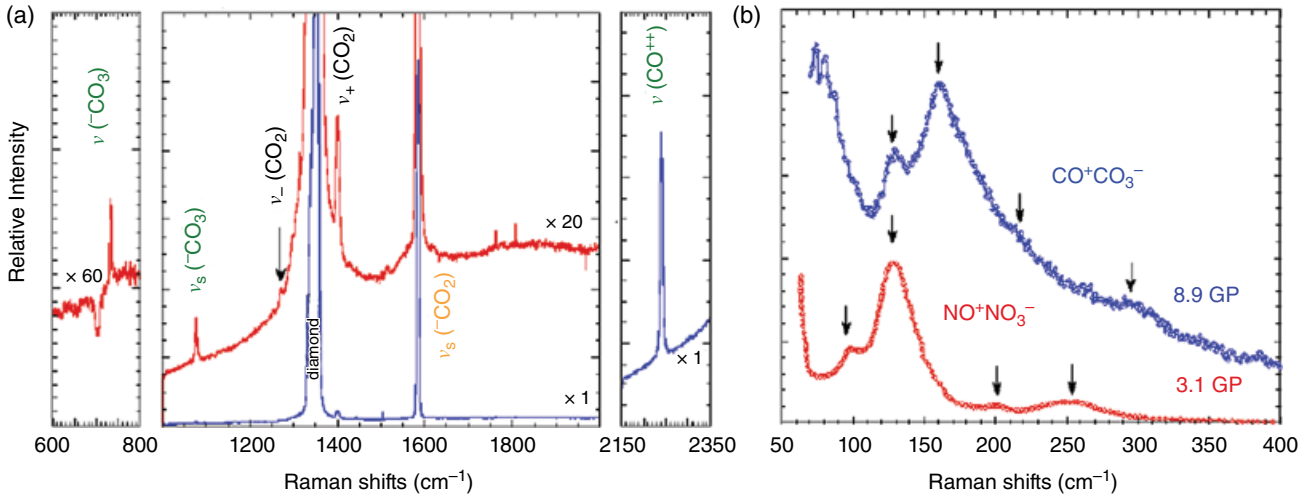

Figure 7.2 Raman spectra of laser-heated C and O_2 mixtures to 2300 K at 10 GPa in the spectral regions for (a) internal vibrations and (b) external lattice modes. It shows the evidences for formation of CO_2 and $COCO_3$ (an ionic form of CO_2 dimer). See electronic version for color representation of the figures in this book.

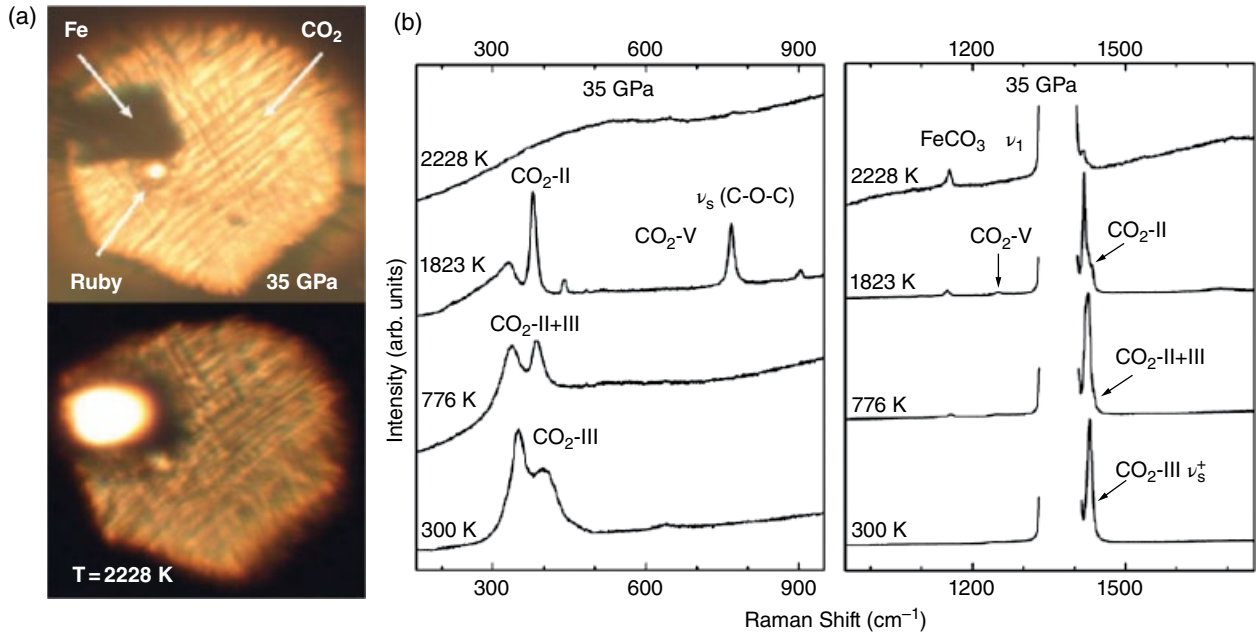

Figure 7.3 (a) Microphotograph of CO_2-Fe samples before (top, at ambient temperature) and during (bottom, at 2228 K) laser heating at 35 GPa in DAC. (b) Raman spectra of laser-heated CO_2 through Fe to 2230 K at 35 GPa, showing the transformation of CO_2-III to CO_2-II, CO_2-V, and $FeCO_3$ as temperature increases. See electronic version for color representation of the figures in this book.

and core. Thus, this result highlights the significant role of extended carbonates in the deep carbon cycle.

7.3.2. Carbonate Formation

The formation of carbonates at high temperatures and low pressures (Figure 7.2) advocates a potential geochemical mechanism of transporting carbonaceous volatiles into deep Earth interiors (Manning et al., 2013). In fact, carbonate minerals (especially of Ca and Mg) are abundant mostly in the Earth's crust (Oganov et al., 2013). To examine the formation of carbonate in deep Earth's mantle, we have investigated the transformation of CO_2 on the presence of Fe abundant in Earth's deeper mantle and core. Figure 7.3a shows the microphotograph of highly strained CO_2-III and Fe samples in DAC, before (top at ambient temperature) and during (bottom at 2228 K) laser heating at 35 GPa. Raman spectra of CO_2 laser heated through Fe were taken at several temperatures at the same pressure, as noted on Figure 7.3b. The results indicate the transformation of CO_2-III to initially CO_2-II at 776 K and then CO_2-V at 1823 K, as well as the formation of siderite $FeCO_3$ at 2228 K. The formation of $FeCO_3$ is apparent from the characteristic vibrational ν_1 peak of carbonate at ~1100 cm^{-1} (Farsang, 2018). Note that the formation of siderite occurs at the onset of the ionization line of CO_2 in Figure 7.1, underscoring the significant role of siderite in the delivery of carbonaceous volatiles deep into the Earth's mantle.

7.3.3. Ionization of XCO_2

The ionic character of the C-O bonds in XCO_2 increases further at high temperatures. Upon laser heating to ~1700–1800 K at 85 GPa, CO_2-V transforms into an extended ionic solid (*i*-CO_2), characterized by four characteristic Raman bands at 2000, 1200, 850, and 400 cm^{-1}, as shown in Figure 7.4a. Note that the systematic of this Raman spectrum is remarkably similar to those of ionic carbonate $COCO_3$ and previously observed ionic nitrate $NONO_3$ (Agnew et al., 1983; Bolduan et al., 1984). However, there are some important differences. For example, both the ν_1 (CO_3) at 980 cm^{-1} and particularly the ν_s (CO) at 1950 cm^{-1} appear at substantially lower frequencies than those of ionic solids at 1070 cm^{-1} and 2220 cm^{-1}, respectively, at ~10 GPa. Nevertheless, extrapolating the pressure dependence of the ν_1 (NO_3) mode to 85 GPa greatly reduces the difference to within 20–30 cm^{-1}, which can easily account for the mass difference. The substantially greater difference in the ν_s(CO) mode cannot be explained in terms of pressure dependence or mass difference, but it may indicate a local structural difference of carbonyl ions in *i*-CO_2 from $COCO_3$.

A plausible model for the large softening of ν_s (CO) mode is an incorporation of CO ions to adjacent carbonate layers. This would then lead to a structure analogous to the theoretically predicted mixed coordinated carbonate structures (Montoya et al., 2008; Sun et al., 2009). Hybridization of this type would certainly soften

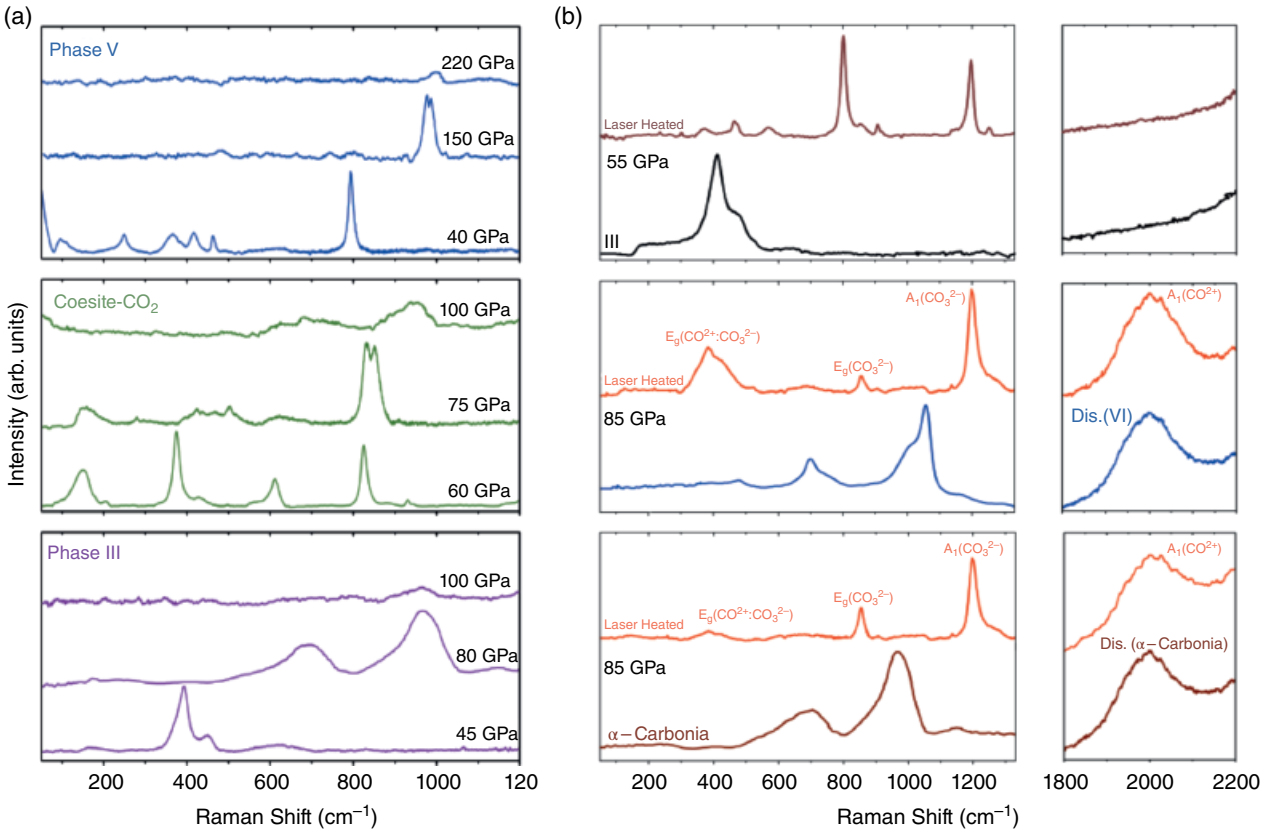

Figure 7.4 (a) Raman spectra of extended carbon dioxide phases before and after laser heating, showing the transformation to extended ionic CO_2 carbonates (*i*-CO_2) at ~85 GPa and 1700–1800 K. (b) Raman spectra of extended carbon dioxide phases to 220 GPa, showing the pressure-induced amorphization of (top) four-fold CO_2-V via new high-pressure phase V′ above 150 GPa, (middle) coesite-CO_2 (*c*-I) via a high pressure-form (*c*-II), and (bottom) phase III via *a*-carbonia, at ambient temperature. See electronic version for color representation of the figures in this book.

ν_s (CO) and ν_1 (CO_3) modes, as observed. In fact, the calculated vibration spectrum shows CO stretching in the range of 1800 to 1900 cm^{-1}, depending on the degree of mixed coordination (Lee et al., 2009; Montoya et al., 2008). On the other hand, it is important to recognize that all calculated structures produce several strong extra bands between 700 and 400 cm^{-1}, which are absent in *i*-CO_2 but present in disordered *a*-carbonia and phase VI. Therefore, the absence of such disordered peaks suggests a fully extended and more ordered *i*-CO_2 structure.

Note that *i*-CO_2 is formed only by heating extended CO_2 solids above 85 GPa; for example, heating phase III at 55 GPa produces only phase VIII (Sengupta & Yoo, 2009), whose Raman spectrum consists of two sharp peaks at 800 and 1200 cm^{-1}, without the presence of the 2000 cm^{-1} peak for CO.

7.3.4. Pressure-Induced Amorphization

Above 40 GPa, carbon dioxide polymerizes to a wide range of covalently bonded extended solids: four-fold CO_2-V (Datchi et al., 2012; Iota et al., 1999; Santoro et al., 2012; Sera et al., 1999; Yoo et al., 2013) and coesite-CO_2 (*c*-CO_2) (Sengupta & Yoo, 2010), pseudo-six-fold CO_2-VI (Iota et al., 2007), and mixed three- and four-fold coordinated *a*-carbonia (Santoro et al., 2006), each with a characteristic Raman-active ν_b (C-O-C) bending vibron at around 700–1000 cm^{-1}. Upon further compression to 100–220 GPa, these XCO_2 phases become nonmetallic amorphous solids, as evident from complete loss of their vibrons and optical transparency. Figure 7.4b shows the corresponding spectral change of CO_2-V to 220 GPa as an example.

Note that pressure-induced amorphization occurs at greatly diverse pressures, depending on extended phases: for example, CO_2-VI at 80 GPa, *c*-CO_2 at 100 GPa, and CO_2-V at 220 GPa. In fact, intermediate phases CO_2-III and CO_2-IV become amorphous solids at substantially lower pressures of 60 and 80 GPa, respectively (Santoro et al., 2006; Yoo et al., 2001). Yet it is remarkable that the pressure-induced amorphization occurs when the ν_b vibron reaches about the same Raman frequency, ~1000 cm^{-1}, well above the ν_b (C-O-C) mode of six-fold configuration (CO_6) at ~900 cm^{-1}. Therefore, it is conceivable that

the amorphization represents a frustration of four-fold coordinated CO4 to increase either the packing density or the coordination number as pressure increases above 100 GPa.

A similar structural frustration or disorder was observed in CO_2-VI, where carbon atoms are surrounded by an average of six oxygen atoms in a highly distorted octahedral with an average C-O distance of 1.45–1.71 Å (Iota et al., 2007), representing a substantial degree of ionic character in C-O bonds. Considering an approximately 10% in Si-O bond length between four-fold quartz (1.61 Å) and six-fold stishovite (1.76–1.81 Å) (Andrault et al., 1998), we speculate that the C-O bond length in CO_2-VI must increase even larger to ~1.65–1.75 Å in order to accommodate six oxygen atoms around relatively small carbon atoms. With further compression, a separation of this size would eventually lead to a structural destruction forming amorphous solid, in which carbon atoms are in highly mixed coordination with six or more nearest neighbor atoms. The driving force is then to increase the packing density, as is apparent from the ν_b mode shifted to ~1050 cm^{-1} (near that of carbonate). Therefore, it seems that the observed pressure-induced amorphization is driven by enhanced ionicity in carbon-oxygen bonds and topological densification.

7.4. DISCUSSION

The stability of CO_2 carbonates (both CO_2-V and *i*-CO_2) over a large pressure-temperature region relevant to the Earth's mantle and core strongly advocates a possibility that volatile carbon dioxide and carbonates are incorporated deep in the Earth's interior. Figure 7.5 supports this conjecture. It provides, for example, some constraints to evaluate the stability of carbonate minerals in descending slabs. It is also relevant to calculate the thermodynamics and phase assemblies associated with chemical reactions such as $MgCO_3 \rightarrow MgO + CO_2$ and $CaCO_3 \rightarrow CaO + CO_2$ (Dasgupta & Hirschmann, 2006). Using the equation of state of extended CO_2-V, for example, it can be readily shown that the mixture of extended CO_2 and MgO is substantially denser than $MgCO_3$ and other silicate minerals and is better matched to the Preliminary Reference Earth Model (PREM) in the upper mantle below 600 km (see Figure 7.5 inset). Therefore, even if $MgCO_3$ dissociates, CO_2 would remain either as extended CO_2-V or *i*-CO_2 in descending slabs, delivering CO_2 deep into the Earth's mantle. A small contribution of iron in $MgSiO_3$ perovskite or postperovskite (Shim, 2008) can compensate for the density difference resulting from the presence of

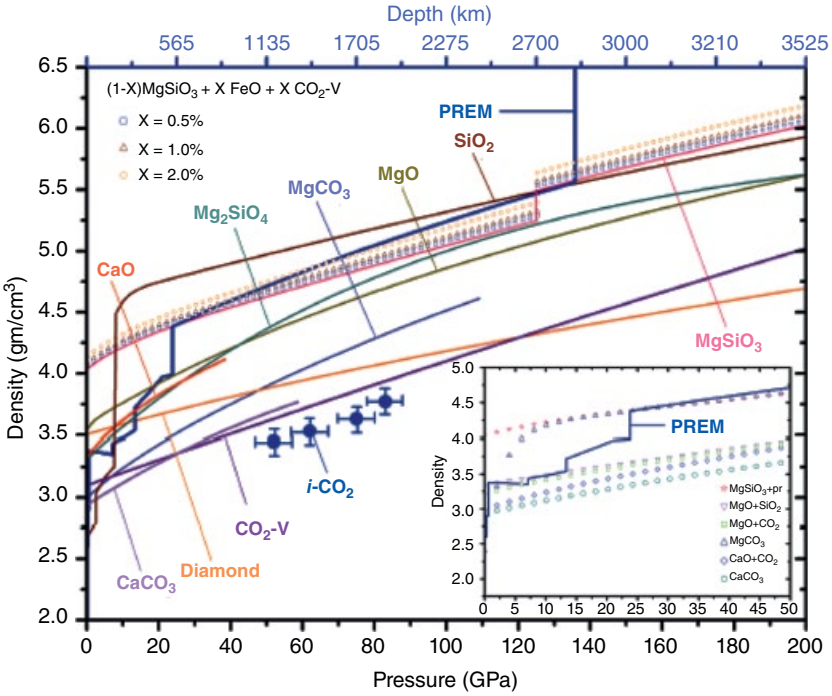

Figure 7.5 The pressure-density plots of various phases of XCO_2 and their analogs (C, $NONO_3$), the major constituents of Earth's mantle ($CaCO_3$, SiO_2, $MgCO_3$, and $MgSiO_3$), and the Preliminary Reference Earth Model (PREM). Also plotted are the calculated densities of a ternary compound of two of the most common minerals in the Earth's core-mantle boundary (perovskite and wustite) and extended CO_2: $(1 - x)MgSiO_3 + xFeO + xCO_2$-V, where x = 0.005, 0.01, and 0.02. The inset also shows the similar density variation of two binary compounds of extended CO_2 with MgO and CaO compared with two common minerals from the Earth's mantle, calcite and magnesite, and highlights the distinct possibility that $MgCO_3$ and $CaCO_3$ exist down to the 560 km transition zone of the Earth's mantle. See electronic version for color representation of the figures in this book.

extended CO_2: $(Mg_{1-x}, Fe_x)(Si_{1-x}, C_x)O_3 = (1 - x)MgSiO_3 + xCO_2 + xFeO$, with $x = 0.5\%$ to 2.0% as it moves deeper into the core-mantle boundary from the 670 km transition zone. The decomposition of XCO_2 phases in the outer core region, then, provides a geochemical mechanism for the presence of deep carbon species (such as Fe_3C) (Li et al., 1996; Nakajima et al., 2009) in the Earth's outer core, originally delivered from CO_2 in the atmosphere.

The P-T-induced transformations of CO_2 can be understood in terms of carbon redox processes that may have important implications to the deep carbon cycle (see Figure 7.6a). For example, the pressure-induced transformations of molecular CO_2 to extended CO_2, covalent or ionic alike, are simply a carbon oxidation process, converting the sp^2 C=O bonds in CO_2 to the sp^3 C-O bonds in orthocarbonates (CO_4) or carbonates (CO_3) of XCO_2 phases. The pressure-induced ionization process, on the other hand, is a reduction process that converts the sp^3 C-O bonds back to the sp^2 C=O in *i*-CO_2 and further in $C+O_2$. Such a reduction process is, then, assisted by high temperature. The rapid temperature rise at the Earth's mantle-core boundary can further accelerate the ionization and decomposition of extended CO_2 or carbonate minerals to form deep carbons and carbonaceous minerals. As such, it gives a rebirth of fully reduced carbon species deep in the Earth's mantle–outer core boundary region, where carbon oxidation can start again as it floats up over a geological time frame.

The pressure-induced transformation in dense CO_2 also highlights several fundamental barochemistry (or pressure-induced solid-state chemistry) concepts, as illustrated in a hypothetical 2D lattice in Figure 7.6b (Yoo, 2017). At low pressures, molecular solids are relatively soft, primarily held by van der Waals interactions. Upon compression, molecular solids transform into extended polymeric structures to soften highly repulsive intermolecular interaction by delocalizing valence electrons or making bonds between nearby molecules (i.e., the pressure-induced electron delocalization). These high-symmetry polymeric structures can further undergo symmetry-breaking distortions (such as Jahn-Teller or Peierls) to enhance their packing efficiencies, which result in low-symmetry distorted or even amorphous structures with highly polarized chemical bonds. Upon further compression, the electrostatic packing energy dominates over the electron hybridization energy, converting these covalent network structures into ionic solids (i.e., pressure-induced ionization) or extended mixtures of constituting elements (phase separation), depending on the chemical/bond/structural miscibility of dense solid interfaces of multiphase and multicomponents. These transformations are strongly controlled by kinetics, giving rise to the path dependence, metastable intermediate states, and near ground-state final products, as observed in CO_2 and many other molecular systems. The collective behaviors of lattice phonons, electrons, and charges in these extended structures, on the other hand, can give rise to novel electro-optical properties such as second harmonic generation (Iota et al., 1999) and high Tc superconductivity (Drozdov et al., 2015).

7.5. CONCLUSION

We have described the transformations of carbon dioxide to extended solids, both covalent and ionic, at high pressures and temperatures. These results suggest the presence of volatile carbon dioxide and carbonates over a wide range of high P-T conditions in deep Earth's mantle, thus providing a geochemical mechanism explaining the origin of deep carbon species in the Earth's core

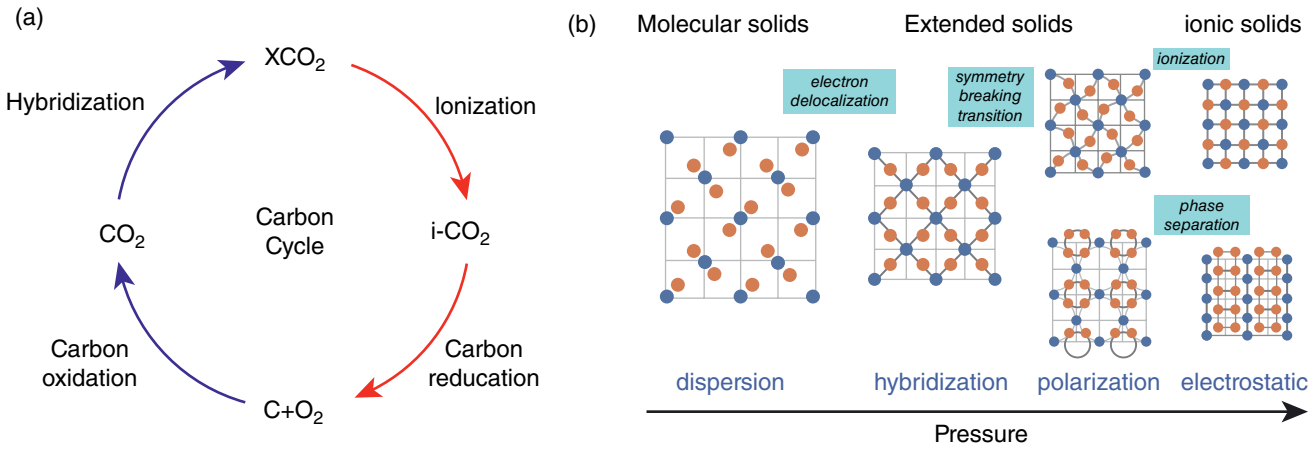

Figure 7.6 (a) A schematic of pressure-induced transformation of solid CO_2 in two dimensions, showing the fundamental concepts of pressure-induced chemistry (or barochemistry), such as the pressure-induced electron hybridization to extended solids and the pressure-induced ionization to ionic solids and decomposition products. (b) A schematic of deep carbon cycle governed by carbon Redox processes at combined high pressures and temperatures. See electronic version for color representation of the figures in this book.

and mantle boundary. In a context of carbon redox chemistry, we have conjectured a deep carbon cycle that may give a rebirth of fully reduced carbon species deep in the Earth's mantle–outer core boundary. We have also discussed fundamental barochemical concepts to explain the pressure-induced transformations in CO_2 and other molecular solids.

ACKNOWLEDGMENTS

This work has been performed in support of the National Science Foundation, Division of Materials Research (Grant No. 1701360), the Department of Energy, National Nuclear Security Administration (DE-NA0003342), the Army Research Office (W911NF-17-1-0468), the donors of the Petroleum Research Fund administered by the American Chemical Society (No. 54806-ND10), and the Sloan Foundation through the Deep Carbon Observatory—Extreme Physics and Chemistry.

REFERENCES

Agnew, S. F., Swanson, B. I., Jones, L. H., Mills, R. L., & Schiferl, D. (1983). Chemistry of nitrogen oxide (N_2O_4) at high pressure: Observation of a reversible transformation between molecular and ionic crystalline forms. *J. Phys. Chem.*, *87*, 5065–5068.

Andrault, D., Fiquet, G., Guyot, F., & Hanfland, M. (1998). Pressure-induced Landau-type transition in stishovite. *Science*, *282*, 720–724.

Bolduan, F., Jodl, H. L., & Lowenschuss, A. (1984). Raman study of solid N_2O_4: Temperature induced autoionization, *J. Chem. Phys. 80*, 1739–1743.

Dasgupta, R., & Hirschmann, M. M. (2006). Melting in the Earth's deep upper mantle caused by carbon dioxide. *Nature*, *440*, 659–662.

Datchi, F., Mallick, B., Salamat, A., & Ninet, S. (2012). Structure of polymeric carbon dioxide CO_2-V. *Phys. Rev. Lett*., *108*, 125701-1-5.

Drozdov, A. P., Eremets, M. I., Troyan, I. A., Ksenofontov, V., & Shylin, S. I. (2015). Conventional superconductivity at 203 kelvin at high pressures in the sulfur hydride system. *Nature*, *525*, 73–76.

Dziubek, K. F., Ende, M., Scelta, D., Bini, R., Mezouar, M., Harbarino, G., & Miletich, R. (2018). Crystalline polymeric carbon dioxide stable at megabar pressures. *Nat. Comm.*, *9*, 3148.

Farsang, S., Facq, S., & Redfern, S.A.T. (2018). Raman modes of carbonate minerals as pressure and temperature gauges up to 6 GPa and 500 °C. *Am. Mineral.*, *103*, 1988–1998.

Hazen, R. M., Jones, A. P., & Baross, J. A. (2013). Carbon in Earth. *Rev. Mineral. Geochem.*, *75*, 1–698.

Iota, V., Yoo C. S., & Cynn, H. (1999). Quartzlike carbon dioxide: An optically nonlinear extended solid at high pressures and temperatures. *Science*, *283*, 1510–1513.

Iota, V., Yoo, C. S., Klepeis, J.-H., Jenei, Z., Evans, W., & Cynn, H. (2007). Six-fold coordinated carbon dioxide VI. *Nature Mater.*, *6*, 34–38.

Isshiki, M., Irifune, T., Hirose, K., Ono, S., Ohishi, Y., Watanuki, T. (2004). Stability of magnesite and its high-pressure form in the lowermost mantle, *Nature*, *427*, 60.

Kampman, N., Bickle, M., Wigley, M., & Dubacq, B. (2014). Fluid flow and CO_2-fluid-mineral interactions during CO_2-storage in sedimentary basins *Chem. Geology*, *369*, 22–50.

Kelemen, P. B., & Manning, C. E. (2015). Reevaluating carbon fluxes in subduction zones: What goes down, mostly comes up. *Proc. Nat. Acad. Sci.*, *112*, E3997–E4006.

Leckner, K. S., 2003. A guide to CO_2 sequestration. *Science*, *300*, 1677–1678.

Lee, M. S., Montoya, J. A., & Scandolo, S. (2009). Thermodynamic stability of layered structures in compressed CO_2. *Phys. Rev. B*, *79*, 144102-1-4.

Li, J., & Agee, C. B. (1996). Geochemistry of mantle-core differentiation at high pressure. *Nature*, *381*, 686–689.

Manning, C. E., Shock, E. L., & Sverjensky, D. A. (2013). The chemistry of carbon in aqueous fluids at crustal and upper-mantle conditions. *Rev. Mineral. Geochem.*, *75* 109–148.

Mao, W. L., Mao, H. K., Eng, P., Trainor, T., Newville, M., Kao, C. C., et al. (2003). Bonding changes in compressed superhard graphite. *Science*, *302*, 425–427.

Mao, H. K., Xu J., & Bell, P. M. (1986). Calibration of the ruby gauge to 800 kbar under quasi-hydrostatic conditions. *J. Geophys. Res.*, *91*, 4673–4676.

Montoya, J. A., Rousseau, R., Santoro, M., Gorelli, F., & Scandolo, S. (2008). Mixed threefold and fourfold carbon coordination in compressed CO_2. *Phys. Rev. Lett*., *100*, 163002-1-4.

Nakajima, Y., Takahashi, E., Suzuki, T., & Funakoshi, K.-I. (2009). "Carbon in the core" revisited. *Phys. Earth and Planet. Inter.*, *174*, 202–211.

Nellis, W. J., Mitchell, A. C., Ree, F. H., Ross, M., Holmes, N. C., Trainor, R. J., & Erskine, D. J. (1991). Equation of state of shock-compressed liquids: Carbon dioxide and air. *J. Chem. Phys.*, *95*, 5268–5272.

Oganov, A. R., Hemley, R. J., Hazen, R. M., & Jones, A. P. (2013). Structure, bonding, and mineralogy of carbon at extreme conditions. *Rev. Mineral. Geochem.*, *75*, 47–77.

Ono, S., Kikegawa, T., Ohishi, Y., & Tsuchiya, J. (2005). Post-aragonite phase transformation in CaCO3 at 40 GPa. *Am. Mineral.*, *90*, 667–671.

Saal, A. E., Hauri, E. H., Langmuir, C. H., & Perfit, M. R. (2002). Vapour undersaturation in primitive mid-ocean-ridge basalt and the volatile content of Earth's upper mantle. *Nature*, *419*, 451–455.

Santoro, M., Gorelli, F. A., Bini, R., Haines, J., Cambon, O., Levelut, C., et al. (2012). Partially collapsed cristobalite structure in the non molecular phase V in CO_2. *Proc. Nat. Acad. Sci.*, *109*, 5176–5179.

Santoro, M., Gorelli, F. A., Bini, R., Ruocco, G., Scandolo, S., & Crichton, W. A. (2006). Amorphous silica-like carbon dioxide. *Nature*, *441*, 857–860.

Schrauder, M., & Navon, O. (1993). Solid carbon dioxide in a natural diamond. *Nature*, *365*, 42–44.

Sengupta, A., Kim, M., Yoo, C. S., & Tse, J. S. (2012). Polymerization of carbon dioxide: a chemistry view of molecular-to-nonmolecular phase transitions. *J. Phys. Chem., C*, *116*, 2061–2067.

Sengupta, A., & Yoo, C. S. (2009). Raman studies of molecular-to-nonmolecular transitions in carbon dioxide at high pressures and temperatures. *Phys. Rev. B*, *80*, 014118-1-6.

Sengupta, A., & Yoo, C. S. (2010). Coesite-like CO_2: an analog to SiO_2. *Phys. Rev. B*, *82*, 012105-1-4.

Sera, S., Corazon, C., Chiarotti, G.L., Scandolo, S., & Tossatti, E. (1999). Pressure-induced solid carbonates from molecular CO_2 by computer simulation. *Science*, *284*, 788–790.

Shim, S.-H., Catalli, K., Hustoft, J., Kubo, A., Prakapenka, V. B., Caldwell, W. A., & Kunz, M. (2008). Crystal structure and thermoelastic properties of $(Mg_{0.91}Fe_{0.09})SiO_3$ postperovskite up to 135 GPa and 2700 K. *Proc. Nat. Acad. Sci.*, *105*, 7382–7386.

Sleep, N. H., & Zahnie, K. (2001). Carbon dioxide cycling and implications for climate on ancient Earth. *J. Geophys. Res,. 106*, 1373–1399.

Sun, J., Klug, D. D., Mortonak, R., Montoya, J. A., Lee, M. S., Scandolo, S., & Tosatti, E. (2009). High-pressure polymeric phases of carbon dioxide. *Proc. Natl. Acad. Sci.*, *106*, 6077–6081.

Yoo, C. S. (2013). Physical and chemical transformations of highly compressed carbon dioxide at bond energies. *Phys. Chem. Chem. Phys.*, *15*, 7949–7966.

Yoo, C. S. (2017). New states of matter and chemistry at extreme pressures: Low-Z extended solid. *MRS Bull.*, *42*, 724–728.

Yoo, C. S., Cynn, H., Gygi, F., Galli, G., Iota, V., Nicol, M. F., et al. (1999). Crystal structure of carbon dioxide at high pressure: "Superhard" polymeric carbon dioxide. *Phys. Rev. Lett.*, *83*, 5527–5530.

Yoo, C. S., Iota, V., & Cynn, H. (2001). Nonlinear carbon dioxide at high pressures and temperatures. *Phys. Rev. Lett.*, *86*, 444–447.

Yoo, C. S., Kim, M., Morgenroth, W., & Liermann, P. (2013). Transformation and structure of silicatelike CO_2-V. *Phys. Rev. B*, *87*, 214103-1-9.

Yoo, C. S., Sengupta A., & Kim, M. (2011). Carbon dioxide carbonates in the Earth's mantle: Implications to the deep carbon cycle. *Angew. Chem. Int. Ed.*, *50*, 11415–11418.

Zhu, Y., & Ogasawara, Y. (2002). Carbon recycled into deep Earth: Evidence from dolomite dissociation in subduction-zone rocks. *Geology Soc. Am.*, *30*, 947–950.